

pubs.acs.org/Biomac Article

Ensemble Force Spectroscopy of a G-Quadruplex Cluster on a Single-Molecule Platform

Pravin Pokhrel,[†] Jiayi Wang,[†] Sangeetha Selvam, Sagun Jonchhe, Shankar Mandal, and Hanbin Mao*



Cite This: Biomacromolecules 2022, 23, 4795-4803



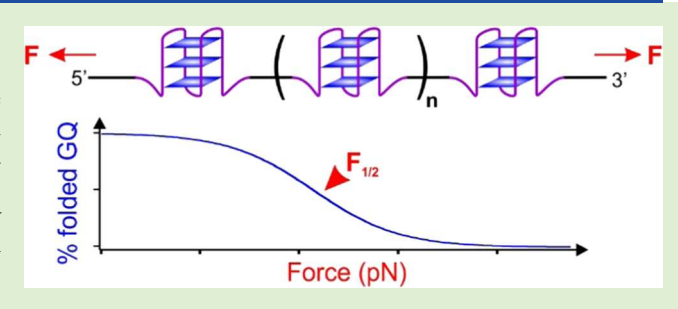
ACCESS I

III Metrics & More

Article Recommendations

s Supporting Information

ABSTRACT: Single-molecule methods offer high sensitivities with precisions superior to bulk assays. However, these methods are low in throughput and cannot repetitively interrogate the same cluster of molecular units. In this work, we investigate a tandem array of G-quadruplexes on a single-molecule DNA template with a throughput of at least two orders of magnitude higher than single-molecule force spectroscopy. During mechanical unfolding by optical tweezers, the array of G-quadruplexes experiences identical force, temperature, and ionic conditions, which not only reduce environmental noise but also render unfolding transitions



indistinguishable among individual G-quadruplexes. The resultant ensemble behaviors are analyzed by scanning force diagrams, which reveals accurate $F_{1/2}$ values, where 50% of G-quadruplexes are unfolded. Independent of the number of G-quadruplexes (n > 15) contained in a cluster, $F_{1/2}$ can effectively evaluate G-quadruplex ligands in a new method called differential scanning forcemetry. When the same G-quadruplex cluster is subject to a series of constant forces in force-jump experiments, unfolding rate constants of G-quadruplexes can be effectively evaluated as a function of force. The high precision demonstrated in all of these measurements reflects the power of repetitive sampling on the same cluster of single-molecule entities under identical conditions. Since biomolecules such as DNA, RNA, and proteins can be conveniently incorporated in a tandem array, we anticipate that this ensemble assay on single-molecule entities (EASE) provides a generic means of ensemble force spectroscopy to amalgamate the accuracy of ensemble measurements with the precision of single-molecule methods.

■ INTRODUCTION

Single-molecule techniques offer sensitivities unparalleled to ensemble average approaches. The superior sensitivity is derived from the capability of measuring single-molecule properties. This single-molecule measurement also renders high sampling precisions. Unlike ensemble average experiments in which the number of analyte molecules is varied significantly in each measurement, such a variation is precisely known in single-molecule measurements. As a result, signal fluctuations due to a different number of analyte molecules can be eliminated in single-molecule measurements, which reduce standard deviations.

Due to the measurement sensitivity, it is convenient for single-molecule techniques to accurately interrogate a localized area or a sample with a small size. However, to render a global picture of an ensemble system, the throughput of single-molecule methods becomes a rate-limiting step. Unlike bulk measurements where average information can be obtained quickly for an ensemble system, it is not feasible to survey a large population if molecules are analyzed one-at-a-time in an experimentally accessible time scale. Another disadvantage is the difficulty in repetitive sampling by single-molecule techniques. After only a few measurements, individual analyte molecules are prone to be photobleached for fluorescence detection or broken in mechanical investigations. The failure of

repetitive sampling renders the procedure tedious. In addition, it increases the measurement noise since the stochastic variation of individual molecules can be exaggerated when experimental conditions change subtly.

A technique with single molecular precision and bulk-level accuracy in ensemble-averaged, high-throughput measurements can offer a hitherto unavailable means to amalgamate the advantages of both approaches. Single-molecule fluorescence has relatively high throughput^{2,3} with respect to force-based methods such as atomic force microscopy (AFM) or optical tweezers.⁴ More than several hundreds of single-molecule entities can be simultaneously measured in a fluorescence imaging frame. However, fluorescence molecules are subject to photodamage, making the repetitive sampling difficult to reduce background noise. In this paper, we proposed and demonstrated ensemble assays of single-molecule entities (or EASE) to drastically increase measure-

Received: August 2, 2022 Revised: October 14, 2022 Published: November 2, 2022





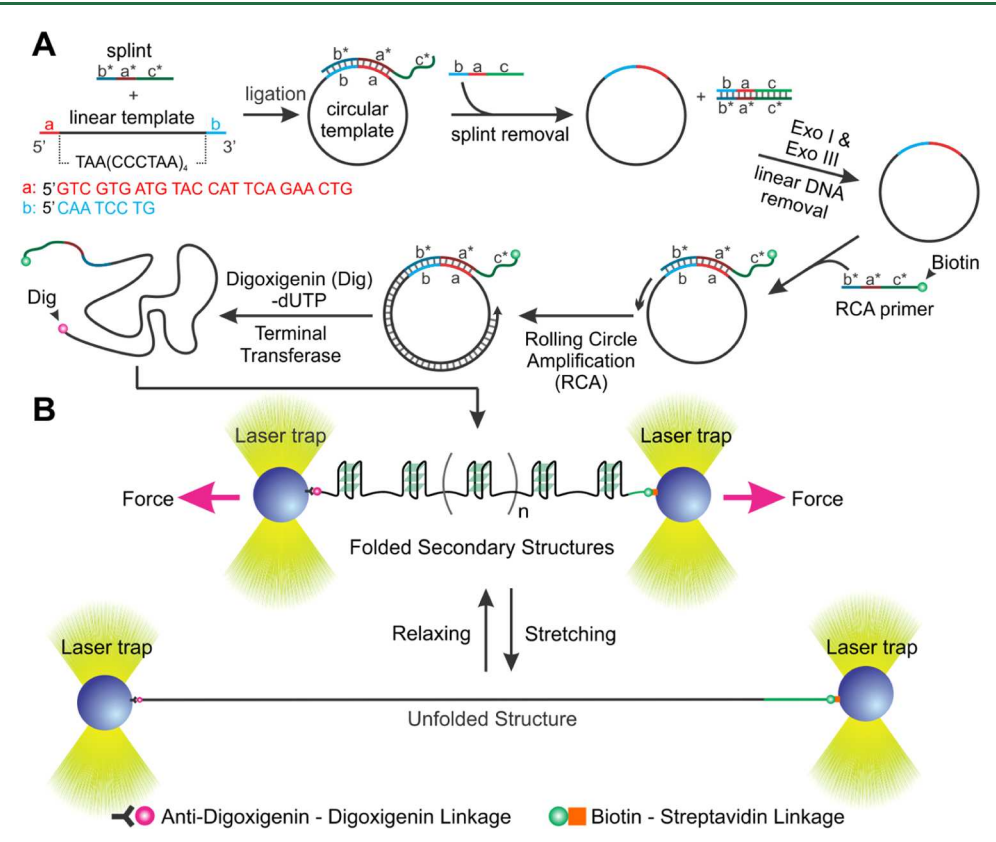


Figure 1. Ensemble assays on an array of human telomeric G-quadruplexes. (A) Rolling circle amplification (RCA) to produce single-stranded DNA repeats of human telomeric G-quadruplex forming sequence. (B) Schematic of scanning force experiments performed in optical tweezers for the RCA-prepared ssDNA template. Potential G-quadruplexes were mechanically unfolded upon stretching. Pink arrows represent the direction at which the force is applied.

ment throughput, as well as to perform repetitive sampling for a cluster of molecular entities. The molecular cluster consists of dozens of identical single-molecule units that behave in an ensemble manner on a single molecular platform. Previously, AFM-based single-molecule force spectroscopy (SMFS) has been used to investigate a few (<12) individual Ig domains in a titin molecule, $^{5-8}$ which is a muscle protein with ~ 300 repeats of Ig domains. Since the AFM tip can pick up any domain in the array, it was difficult to cover the full length of the array. To precisely control the number of Ig domains in the protein, molecular biology methods were used to modify the ends of the array for attachment. However, only a limited number of Ig domains can be precisely incorporated probably due to the limitation in protein engineering. Later, optical¹⁰ and magnetic tweezers¹¹ were also used to study the Ig domains in titin. Compared to optical tweezers, magnetic tweezers offer increased throughput owing to their parallel nature to accommodate many single-molecule templates simultaneously. 12-14 Aided by innovative molecular biology approaches, our EASE platform can host hundreds or even more structural units in a single DNA template. Like a container that holds a massive number of molecules for repetitive chemical or physical measurements at the bulk level, such an EASE platform can be considered as a molecular container with zeptoliter volume for repetitive sampling.

To demonstrate that EASE can perform ensemble force spectroscopy in an accurate and high-throughput manner, we used an array of G-quadruplexes as a proof-of-concept example. G-quadruplexes are stable DNA secondary structures formed in guanine (G) rich sequences in promoter regions and

telomeres, ¹⁵ as well as at mitotic and meiotic double-strand break (DSB) sites with biological functions involved in various diseases such as cancers. ¹⁶ The EASE approach can perform a rapid evaluation of G-quadruplex ligands that may modulate biological functions of G-quadruplexes from a unique perspective of mechanical stabilities. The EASE expands force spectroscopy at the level of a single or a few units ^{5–7} to the ensemble level that contains hundreds or even more units tandemly arranged in a cluster. Such a cluster ensures the experience of identical force, temperature, and chemical environment for individual units, thereby increasing the signal-to-noise level. Due to the generic feature of the EASE method, we anticipate that EASE can be widely applicable to protein and RNA structures as well.

■ EXPERIMENTAL SECTION

Materials. All DNA oligonucleotides used in this research were purchased from Integrated DNA Technologies (IDT, IA). Their sequences can be found in the Supporting Information, Table S2. Enzymes were purchased from New England Biolabs (NEB, England). Polystyrene beads (streptavidin-coated and anti-digoxigenin antibody-coated) used for trapping in optical tweezers were purchased from Spherotech (Lake Forest, IL). All chemicals and reagents were purchased from Sigma-Aldrich or Fisher Scientific, unless otherwise stated, and were used without further purification.

Synthesis of a Single-Molecule Construct Containing Tandem Array of G-Quadruplex Forming Sequence. To prepare a tandem array of human telomeric G-quadruplexes, we first designed a linear ssDNA template with a sequence (Figure 1A, black) reverse complementary to the G-quadruplex forming sequence flanked by sequences a (red) and b (blue) at the 5' and 3' ends, respectively. We annealed this linear template with a splint fragment,

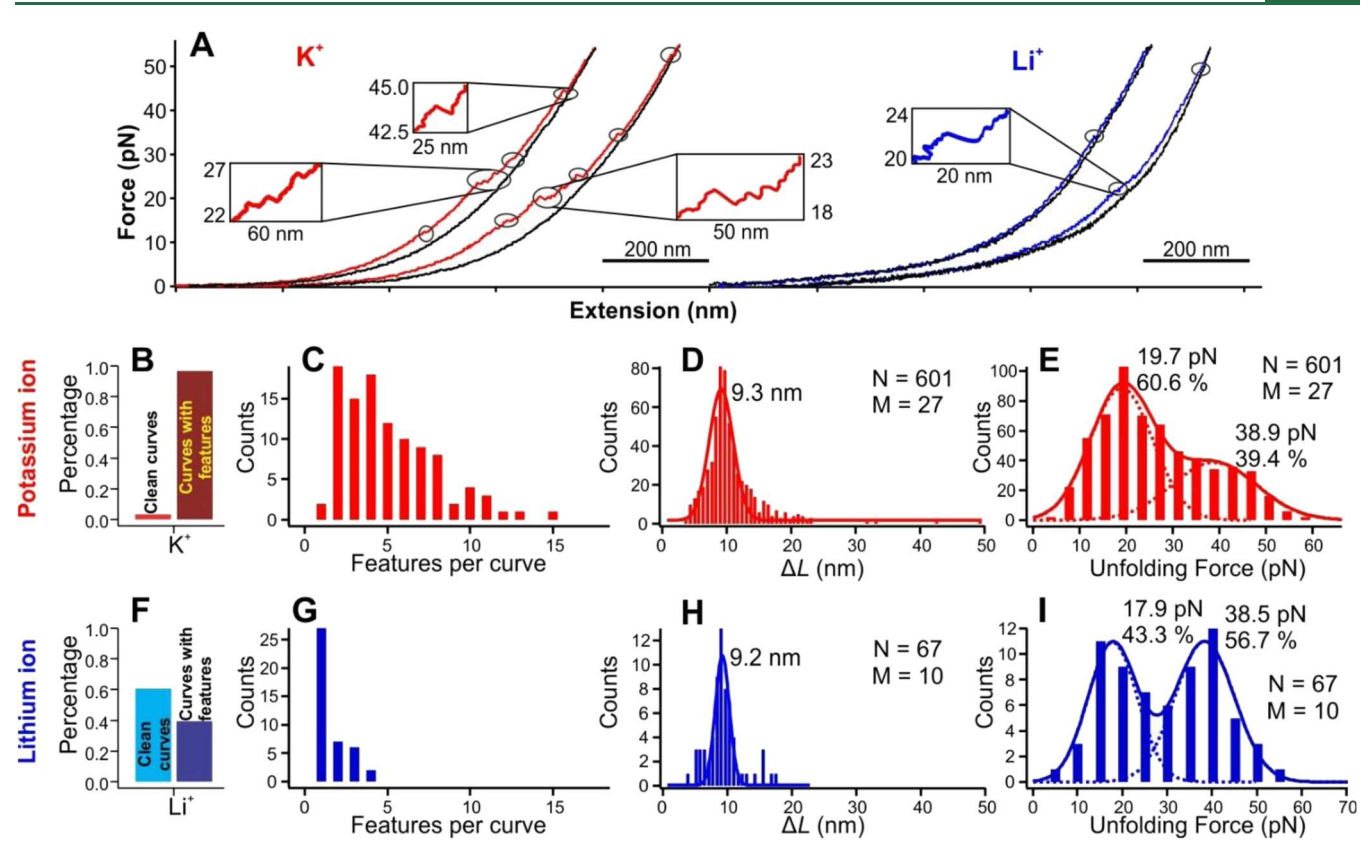


Figure 2. Mechanical properties of individual G-quadruplexes in a cluster. (A) Typical force—extension (F-X) curves obtained during the scanning force experiments on short RCA G-quadruplex constructs (number of G-quadruplex unfolding features n < 15) with multiple unfolding events (circled), representing the unfolding of individual G-quadruplexes in a 10 mM Tris buffer at pH 7.4 with 100 mM K⁺ (red) or 100 mM Li⁺ (blue). The black curves represent relaxing curves. N and M depict the number of data points (unfolding features) and the number of molecules, respectively. The corresponding data analyses were plotted in panels (B)—(E) for the K⁺ buffer and in panels (F)—(I) for the Li⁺ buffer. (B, F) Probabilities of F-X curves with and without G-quadruplex unfolding features, (C, G) histograms of features per curve, (D, H) change-in-contourlength, and (E, I) unfolding force. All experiments were performed at room temperature with 5.5 pN/s loading rate, unless otherwise stated.

5'-c*a*b*, which allowed circularization of the template by T4 DNA ligase. The splint was then removed with a DNA fragment, 5'-bac, which was reverse complementary to the splint sequence. Any noncircularized DNA fragments were subsequently removed by *ExoI* and *ExoIII* nucleases. To obtain the repeats of G-quadruplex forming sequences, we performed rolling circle amplification (RCA)^{17,18} by Phi29 polymerase using a biotinylated primer, 5'-biotin-c*a*b*, against the circularized DNA template. Finally, the 3' end of the RCA product was modified with digoxigenin (Dig) by terminal transferase (see SI Section S2 for details).

Single-Molecule Force Spectroscopy of Tandem Array of G-Quadruplex. We used dual-trap optical tweezers to study force spectroscopy of the construct.¹⁹ Details of the instrumentation are described in our previous publication.²⁰ In brief, a construct is tethered between the two optically trapped polystyrene beads. The end-labeled RCA product enabled the tether formation between two optically trapped beads through biotin-streptavidin and digoxigeninanti-Dig antibody linkages. The tethered DNA construct was subject to force ramping experiments in an optical tweezers instrument.²¹ A tension is developed on the construct when one of the beads is moved apart, which is recorded on a real-time force-extension curve. On stretching the tethered DNA construct, the G-quadruplex structures could be mechanically unfolded when the tension was sufficiently high. Upon relaxing the tethered DNA, the structures could be refolded. The stretching-relaxing processes were reiterated on the same DNA template until the tether was broken. This allowed analyzing mechanochemical properties of multiple DNA structures (i.e., G-quadruplexes in our case) contained in the same DNA construct.

■ RESULTS AND DISCUSSION

Formation of Tandem G-Quadruplexes in the RCA Construct. Apart from the G-quadruplex forming sequence, a 32 nt spacer was introduced to minimize the interaction between neighboring G-quadruplexes in the RCA product (Figure 1A, see sequences a and b). The GO forming sequence in the template was flanked by a 16 nt random sequence on each end, which was replicated many times during the RCA process. To test whether G-quadruplexes were formed in the RCA product, multi-G-quadruplex forming sequences were tethered between two optically trapped beads in a 10 mM Tris buffer (pH 7.4) containing 100 mM KCl, which is known to favor the folding of G-quadruplex. 22,23 Scanning force experiments (Figure 2) revealed unfolding events of multiple G-quadruplex structures in each F-X curve. This was also confirmed by circular dichroism spectra, where we tested our multi-GQ forming RCA products under both K+ and Li+ conditions (see SI Section S11). The characteristic CD signals of crests and troughs confirm the formation of G-quadruplexes in our RCA templates. The CD spectrum of the construct in the presence of 100 mM K⁺ clearly shows three peaks at 205, 250, and 295 nm and two troughs at 220 and 275 nm. These features are consistent with characteristic features of the antiparallel G-quadruplex conformation in literature studies, 24,25 which proves the presence of GQs in the RCA constructs. In the case of Li+, these peaks and troughs are significantly different, which suggests that the GQ structures

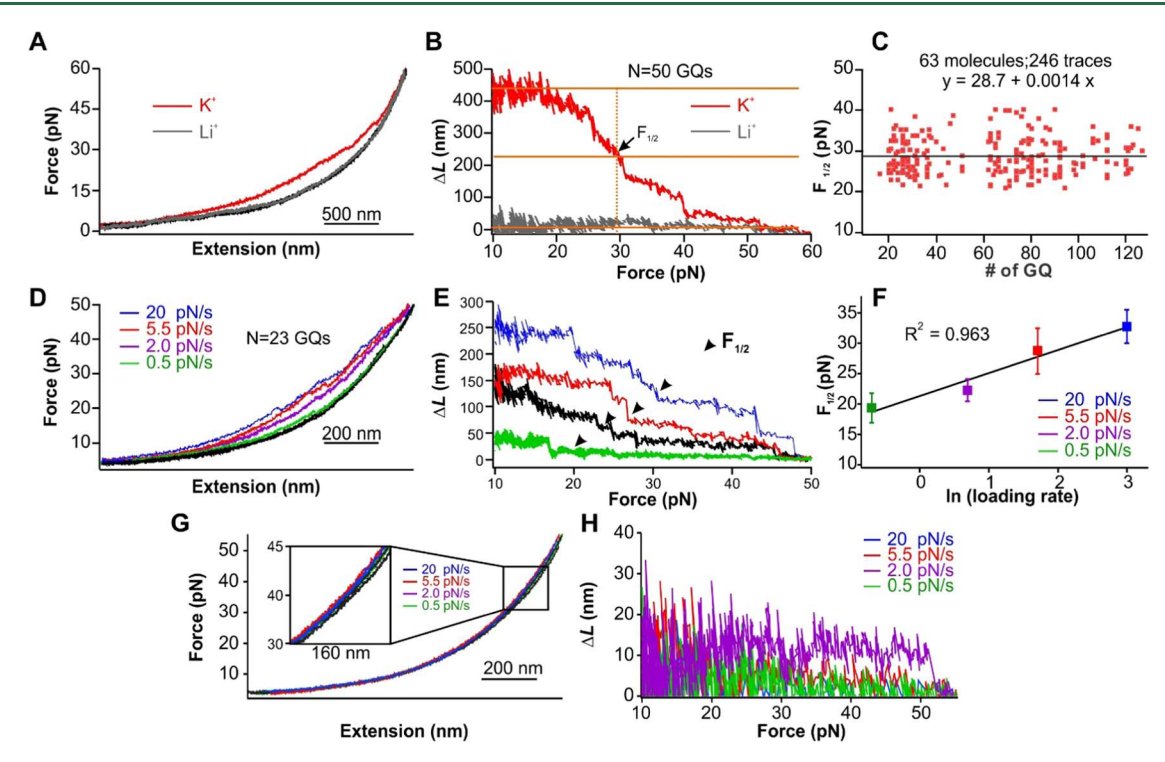


Figure 3. Scanning force diagrams of G-quadruplex clusters. (A) Force–extension curves of long RCA G-quadruplex constructs (the number of G-quadruplex unfolding events >15) obtained with a loading rate of 5.5 pN/s. (B) ΔL vs force curves (scanning force diagrams) of the RCA constructs obtained in a 10 mM Tris buffer (pH 7.4) supplemented with 100 mM KCl (red) or 100 mM LiCl (gray). $F_{1/2}$ at which 50% of structures are mechanically unfolded was depicted by an arrow. (C) $F_{1/2}$ is independent of the number of G-quadruplexes contained in each RCA product (n > 15). (D) Force–extension curves, (E) ΔL vs force curves, and (F) $F_{1/2}$ vs loading rate of the RCA constructs with four different loading rates (0.5–20 pN/s) in the 10 mM Tris buffer supplemented with 100 mM KCl at pH 7.4. (G) Force–extension curves and ΔL –force curves (H) of the RCA constructs with four different loading rates (0.5–20 pN/s) in a 10 mM Tris buffer supplemented with 100 mM LiCl at pH 7.4.

are compromised. Similarly, we also performed a control experiment by replacing the GQ forming sequence in the template with the poly(deoxyadenosine) (dA_{45}) sequence that is not expected to form secondary structures. In the presence of 100 mM KCl, scanning force experiments indeed revealed no secondary structures were formed in the F-X curves (see SI Section S13). This result further supported that the observed unfolding features are due to rupture events of G-quadruplexes.

In the scanning force microscopy experiments, it is noteworthy that when the RCA product was short (unfolded G-quadruplexes n < 15, see SI Section S8 for the determination of the number of GQs in an RCA template), individual unfolding features were obvious. These individual features became indistinguishable when RCA products were long (unfolded G-quadruplexes n > 15, see Figure 3 below), which is a major limitation of this approach. To confirm whether these distinct unfolding features were due to the G-quadruplex unfolding, we first analyzed the short RCA products with less than 15 unfolding features.

Most unfolding features had a change-in-contour-length (ΔL) of ~9.3 nm (Figure 2D,H), which is expected for the unfolding of individual telomeric G-quadruplexes (see refs 22 and 23 and the SI for calculations). Some events with longer ΔL may be due to simultaneous unfolding of multiple G-quadruplex structures or higher-order structures. However, given the finding of a beads-on-a-string pattern without higher-order structures in a telomeric overhang with a native spacer (5'-TTA) between neighboring G-quadruplexes, higher-order structures are unlikely in current sequences with a much

longer 32 nt spacer between adjacent G-quadruplexes.²¹ We observed two unfolding populations centered at 19.7 and 38.9 pN (Figure 2E). While the 19.7 pN population is consistent with the unfolding force of a hybrid-1 G-quadruplex,²⁹ the 38.9 pN species could be a different G-quadruplex conformation, a G-quadruplex stabilized by the quadruplex—quadruplex interactions,³⁰ or another secondary structure. As a control, in a 10 mM Tris buffer with 100 mM LiCl, very few unfolding events were observed (compare Figure 2F,G vs Figure 2B,C, respectively). As stable G-quadruplex conformation is unfavorable in Li⁺ ions,^{31,32} this experiment confirmed the formation of G-quadruplexes in the tandem repeats of telomeric G-quadruplex forming sequences. It is noteworthy that the properties of these rarely formed G-quadruplexes in the Li⁺ buffer can only be revealed in the presence of many G-quadruplex forming units in the RCA construct.

Close inspection on the mechanical unfolding in the presence of Li⁺ revealed that even though Li⁺ ions reduced the folding probability of G-quadruplex, they relatively favored more stabilized G-quadruplexes (Figure 2I, 17.9 pN (43.3%) vs 38.5 pN (56.7%)). This result indicates that the higher force population has less dependency on the Li⁺ ions. Given that the detrimental effect of Li⁺ comes from the metal coordination between G-quartets, ^{33,34} we argue that extra stabilization in the 38.5 pN species could come from the loop—loop interactions ³⁵ or other stabilization structures rather than the coordination of the Li⁺ ions between G-quartets.

When we interrogated longer RCA products (G-quadruplex unfolding events n > 15, see SI Section S8 for the

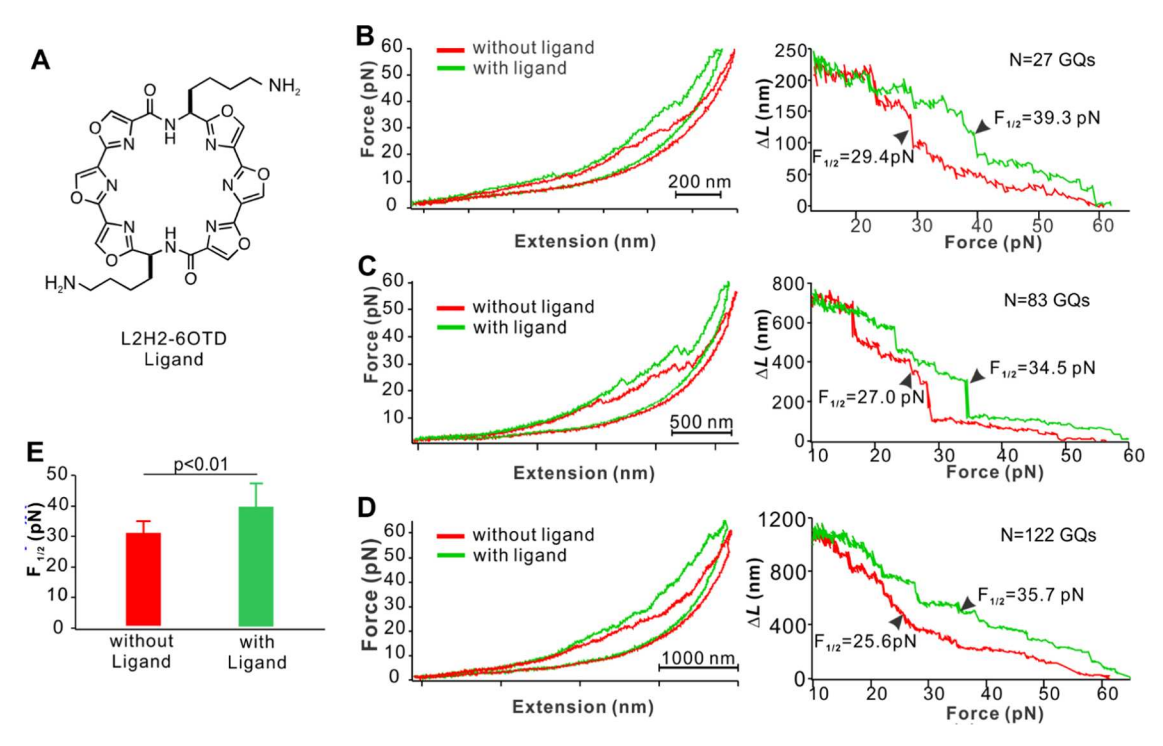


Figure 4. Repetitive sampling yields high accuracy in a differential scanning force diagram to evaluate G-quadruplex (GQ) ligands. (A) Structure of the L2H2-6OTD ligand. (B–D) Force—extension curves (left panels) and corresponding scanning force diagrams (right panels) of the same cluster of G-quadruplexes (n = 27, 83, and 122 GQs in panels (B)–(D), respectively) without (red) and with (green) 100 nM ligand in 10 mM Tris buffer (pH 7.4) supplemented with 100 mM KCl. (E) Average $F_{1/2}$ without and with ligand. A total of 4 molecules with 23 F–X curves were collected to calculate each $F_{1/2}$.

determination of the number of G-quadruplexes in an RCA template), we found that individual unfolding features were no longer distinguishable. As more G-quadruplexes were formed in longer RCA products, it had increased the opportunity to mechanically unfold G-quadruplex units simultaneously. A similar scenario occurs in bulk experiments in which behaviors of individual molecules can no longer be resolved. Instead, average information on an ensemble set of molecules is obtained in bulk assays. In particular, our mechanical unfolding experiments on a cluster of G-quadruplexes resemble thermal melting of folded structures at the bulk level. In a scanning temperature diagram, the percentage of folded structures is plotted against temperature to identify the melting temperature $(T_{\rm m})$, which is defined as the temperature at which 50% of structures are melted. Likewise, if the number of intact Gquadruplex structures in a cluster is plotted against mechanical force in a scanning force diagram, we should be able to retrieve an ensemble unfolding force, $F_{1/2}$, which represents the force at which 50% of structures are mechanically unfolded.

Scanning Force Diagram of Tandem G-Quadruplexes. We rationalized that as more G-quadruplexes are unfolded to ssDNA, the construct becomes longer, which increases apparent change-in-contour-length (ΔL) of the RCA template (see SI Sections S7–S9 for details). Therefore, by calculating ΔL throughout the entire scanning force range, we can follow unfolded G-quadruplexes vs force. To establish such a scanning force diagram, we converted F-X curves to $\Delta L-F$ plots³⁶ by comparing the stretching and relaxing F-X curves at the force regime in which G-quadruplexes started to unfold (>10 pN, 23 see the SI for detailed conversion). We first constructed $\Delta L-F$ curves with 100 mM K⁺ or Li⁺ (Figure 3B). In the presence of K⁺, we observed that G-quadruplexes

maintained a maximum ΔL level at 10-20 pN and started to unfold at >20 pN. At >50 pN, ΔL is reduced to 0, indicating all G-quadruplexes were mechanically unfolded, resulting in complete overlap between the stretching and relaxing F-Xtraces. By extrapolating the plateau regions of the maximal ΔL and $\Delta L = 0$, respectively, we identified the $F_{1/2}$ for this particular construct (n = 50 G-quadruplexes, Figure 3B) as 29.6 pN. This $F_{1/2}$ is located in the middle of the transition region of the ΔL -F traces. It is also close to the average unfolding force of the G-quadruplexes in shorter RCA templates (average force = 29.3 pN in Figure 2E). Both results confirm the accuracy of our $F_{1/2}$ calculation. When we plotted the ΔL vs F curve in the presence of 100 mM Li⁺ (Figure 3B), we observed no unfolding transition. This was expected as Li⁺ destabilizes G-quadruplexes (Figure 2 and refs 29 and 30). To evaluate the effect of the number of Gquadruplexes on the $F_{1/2}$ measurement, we varied the RCA products that contained 16-130 G-quadruplexes. As shown in Figure 3C, the $F_{1/2}$ is independent of the number of Gquadruplexes formed in the constructs (average $F_{1/2} = 28.7$ pN; sd = 4.4 pN; range = 21.0-40.3 pN), reflecting the accurate $F_{1/2}$ measurements when more than 15 Gquadruplexes were sampled together in this ensemble force spectroscopy approach.

Next, we measured $F_{1/2}$ of G-quadruplex clusters (n > 15 G-quadruplexes) under different loading rates (0.5, 2.0, 5.5, and 20.0 pN/s) of mechanical unfolding. In the presence of 100 mM K⁺ (Figure 3D–F), increasing loading rate increased $F_{1/2}$ values, which indicates that under these loading rates, unfolding of G-quadruplexes is a kinetic process (i.e., forceassisted unfolding 37) away from thermodynamic (spontaneous) unfolding equilibrium. Consistent with this kinetic

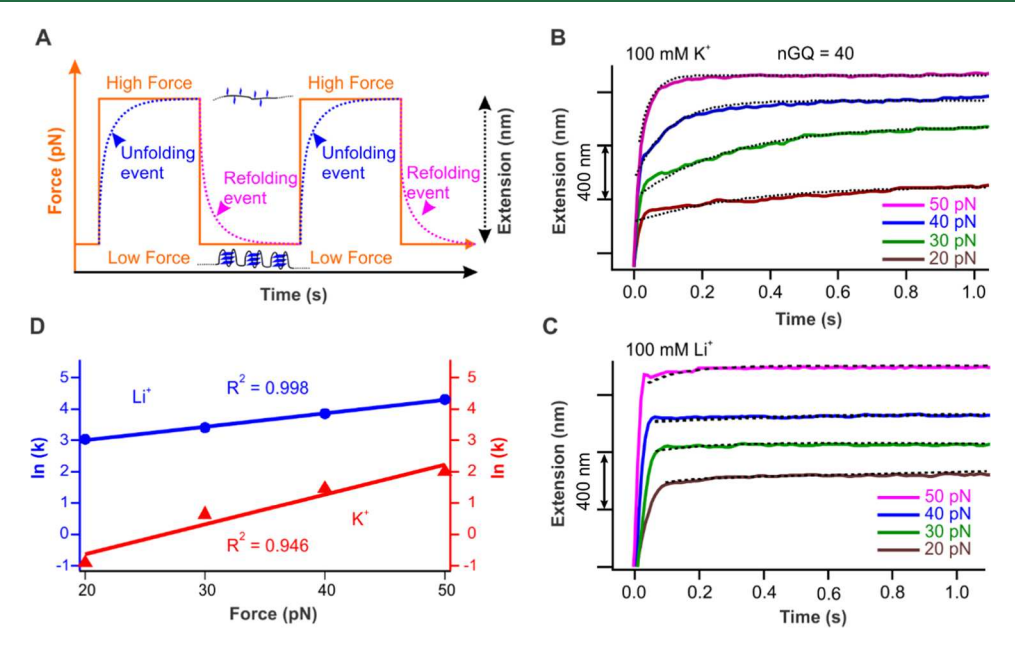


Figure 5. Force-dependent unfolding kinetics of a cluster of G-quadruplexes. (A) Schematic of constant force experiment to retrieve the unfolding kinetics of G-quadruplexes (n > 15) contained in an RCA construct. At low force (~ 0 pN), the G-quadruplexes are folded. When the force is suddenly increased to a constant value, the structures start to unfold, as illustrated by blue dotted curves. This unfolding process can be repeated after refolding of G-quadruplexes as shown by the pink dotted curves. Typical unfolding curves from an RCA construct that contains 40 G-quadruplex repeats at different forces (20-50 pN) in a 10 mM Tris buffer at pH 7.4 supplemented with 100 mM KCl (B) or LiCl (C). The black dotted curves depict single exponential fitting (see the SI for the equation). (D) Natural logarithm of average unfolding rate constants (k) from three different clusters of human telomeric G-quadruplexes vs force in the Tris buffer (pH 7.4) containing 100 mM KCl (red) or LiCl (blue) at different constant forces (20-50 pN). Standard deviations in D are smaller than the size of data points.

force-assisted unfolding regime, the G-quadruplex had an increased opportunity to unfold at lower force when loading rates were decreased. As a result, the maximal ΔL plateau at \sim 10 pN became smaller at the lower loading rates (Figure 3E). In contrast, in the presence of 100 mM Li⁺, the unfolding transition was absent due to insufficient G-quadruplex formation in this buffer, regardless of loading rates (Figure 3G,H). Using the Evans model,³⁷ we calculated the transition distance (x^{\dagger}) from folded telomeric G-quadruplex to the transition state by plotting $F_{1/2}$ with natural logarithm of the loading rate (Figure 3F, see SI Section S5 for equation). This plot was fit well by a linear equation ($R^2 = 0.963$), from which we retrieved x^{\dagger} of 1.1 nm (see Supporting Information). This value is close to the upper range obtained from the unfolding force histograms of individual telomeric G-quadruplexes (x^{\dagger} ranging from 0.8^{38} to 0.45 nm³⁹). It is noteworthy that $F_{1/2}$ from all loading rates could be collected from only one RCA construct (see Figure 3D,E for an example) in which the same set of G-quadruplexes was sampled repeatedly. This resampling feature increased the accuracy as well as the precision of the $F_{1/2}$ determination.

To demonstrate that repetitive sampling can be used to evaluate G-quadruplex ligands, we compared $F_{1/2}$ values for the same set of G-quadruplexes with and without ligand L2H2-6OTD (Figure 4). L2H2-6OTD is a derivative of 6OTD series ligands with an amine group on the side chain that is well-known to strongly interact with a Telo-4G sequence. In the presence of 100 nM L2H2-6OTD (Figure 4A), we observed that force—extension curves at a loading rate of 5.5 pN/s were always located to the left of those obtained from the same G-quadruplex cluster without ligands (Figure 4B—D left). These indicated that the G-quadruplexes were not fully unfolded likely due to bound L2H2-6OTD ligands. When

we combined the two scanning force diagrams in a plot of differential scanning forcemetry (Figure 4B-D right), it is obvious that $F_{1/2}$ was significantly higher when ligands were bound to G-quadruplex (38.1 \pm 6.7 vs 29.2 \pm 2.5 pN, Figure 4E) with p < 0.01 (two tailed t-tests). When comparing RCA constructs with different lengths (Figure 4B-D), we found that the number of G-quadruplexes (n > 27) did not affect $F_{1/2}$ values, which was consistent with the ensemble nature of the G-quadruplex cluster revealed in Figure 3C (n > 15). Strikingly, among four different G-quadruplex clusters tested, each differential scanning force diagram demonstrated higher $F_{1/2}$ in the presence of L2H2-6OTD than that without ligand. This high consistency suggests that only one scanning force experiment is needed to evaluate the binding of the L2H2-6OTD ligand to the G-quadruplex cluster, which requires only a few minutes to obtain $F_{1/2}$. In comparison, it requires many hours to obtain $T_{\rm m}$ in conventional UV melting experiments. These results clearly demonstrated the power of the EASE to evaluate ligands accurately and rapidly for G-quadruplex binding. We name this technique differential scanning forcemetry in analogy to the differential scanning fluorimetry method,41 in which ligand binding to biomolecules is monitored by fluorescence signals in thermal melting procedures.

Ensemble Unfolding Kinetics Revealed by Repetitive Sampling of a Cluster of G-Quadruplexes. To investigate unfolding kinetics of structures at a constant force, the force will be rapidly set to allow the structure to unfold, from which the unfolding rate is determined (Figure 5A). Due to the stochastic nature of single molecules, unfolding occurs randomly even when the force is lower than the average force to unfold the structure. To obtain accurate unfolding time measurement, therefore, a large set of molecular

structures should be tested one-by-one for average results, which makes the whole process tedious. Hundreds of G-quadruplex units in a single-molecule RCA product offer an opportunity to streamline the kinetic measurement with hundred times faster in throughput. To demonstrate this feature, we first subjected a single-stranded RCA product with multiple repeats of G-quadruplex forming sequences to a desired unfolding force within 10 ms (see an ssDNA with n=40 G-quadruplexes in Figure 5B). Unfolding of G-quadruplexes at this force led to increased extension of the ssDNA strand (Figure 5B,C). The extension vs time traces was fitted by a single exponential function (see SI Section S12 for equation). Given that folding is negligible at force >10 pN, such a fitting allowed us to retrieve the unfolding rate constants directly.

Comparing unfolding kinetics between K^+ (Figure 5B) and Li^+ (Figure 5C), we found that multi-G-quadruplexes reached the unfolded state ~ 10 times faster in the Li^+ solution (Figure 5D). This is again consistent with the fact that very few G-quadruplexes exist in the Li^+ solution. Therefore, the kinetics measured in Li^+ buffer likely depicted the mechanical response of the ssDNA backbone to the sudden force jump (Figure 5C). The 10 times difference between the extension rate in the ssDNA backbone and the G-quadruplex unfolding rate also indicated that unfolding rates of multiple G-quadruplexes in the K^+ solution were not influenced by the response of the DNA backbone to external forces.

Not only did the throughput increase by two orders of magnitude, the random noise of the measurement was also drastically reduced since the same G-quadruplex cluster was interrogated repeatedly under almost identical conditions, i.e., force, temperature, and solution, for each G-quadruplex in the cluster (Figure 5B,C). This reduced the variation among different G-quadruplex units when they are investigated one-at-a-time. The decreased noise level is manifested by the small standard deviations of the average unfolding rate constants obtained from three clusters of G-quadruplexes (Figure 5D, the error bars are smaller than the size of the data points).

Next, we estimated the transition distance (x^{\dagger}) from folded telomeric G-quadruplex to the transition state by plotting natural logarithm of average k_{unfold} vs constant force (Figure 5D, see SI Section S5 for the details and equations). These plots showed excellent linear fitting ($R^2 = 0.946$ and 0.998 for 100 mM K⁺ and Li⁺ solutions, respectively). Using the Bell model, ⁴² we retrieved x^{\dagger} of 0.4 nm from the slope of the linear fitting of the plot obtained in the K+ solution (see the Supporting Information). This value falls in the lower range obtained from the unfolding force histograms of individual telomeric G-quadruplexes (0.8 38 to 0.45 nm 39). It is about \sim 2 times difference compared to the x^{\dagger} obtained from the loading rate measurement (Figure 3), which may be ascribed to the different measurement approaches used in these two assays. However, since the loading rate can be different at higher force range due to the constant rate of trap distance displacement used in our experiment, we argue that the force-jump method of determining the x^{\dagger} is more accurate since there is no influence of loading rate on the unfolding of G-quadruplexes.

A similar force-jump approach can also be used to investigate the formation kinetics of G-quadruplex or other DNA secondary structures. In this case, the force is first maintained at a high value to populate unfolded secondary structures. Then, the force can be rapidly (in milliseconds⁴⁴)

jumped to a lower force at which folding of the secondary structures can be followed in real time.

Although the EASE approach can increase throughput about 2–3 orders of magnitude compared to single-molecule force spectroscopy, 5–7 it has reduced resolution on individual units. For example, it has compromised resolution on the mechanical property or dynamic information for individual units in a cluster, which is a common problem in ensemble-based approaches.

CONCLUSIONS

In summary, we have transformed single-molecule force spectroscopy into ensemble force spectroscopy (EFS) with at least 2 orders of magnitude faster in throughput. By collecting data on an ensemble set of single-molecule G-quadruplex structures, EFS allowed us to obtain accurate $F_{1/2}$ values at which 50% of G-quadruplexes was mechanically unfolded. The measurement can be accomplished after only one cycle of force ramping procedure within minutes instead of days required to construct an unfolding force histogram in single-molecule force spectroscopy. Such $F_{1/2}$ was independent of the number of Gquadruplex contained in the RCA construct (n > 15). The $F_{1/2}$ was used to rapidly evaluate the binding capability of Gquadruplex ligands via differential scanning forcemetry. By the unique feature of repetitive sampling on the same cluster of Gquadruplexes, we were able to simultaneously vary loading rates or constant forces on every G-quadruplex in the cluster. Since all G-quadruplexes in the same cluster experienced identical conditions in these experiments, the signal-to-noise levels in these measurements were high. Given the readily available molecular biology techniques to introduce tandem arrays of DNA, RNA, or protein structures, we anticipate that this ensemble assay on single-molecule entities (EASE) represents a generic tool for accurate and high-throughput investigations on various biomacromolecules from the mechanical perspective with single-molecule precision.

ASSOCIATED CONTENT

Supporting Information

The Supporting Information is available free of charge at https://pubs.acs.org/doi/10.1021/acs.biomac.2c00959.

Materials; synthesis of the RCA-based construct; loading rate experiments in optical tweezers; constant force experiments in optical tweezers; calculations using the Bell's model and Evans model; change-in-contour-length of a single unit G-quadruplex; change-in-contour-length of an ensemble set of G-quadruplexes, determining the number of G-quadruplexes in the single-molecule construct; conversion of F-X curves into $\Delta L-F$ curves; calculation of $F_{1/2}$ from ΔL vs F curves; CD spectra of multi-GQ RCA construct; exponential function to fit extension vs time traces; typical F-X curves of a non-GQ forming sequence in the potassium condition; and a list of DNA oligonucleotides used in this study (PDF)

AUTHOR INFORMATION

Corresponding Author

Hanbin Mao — Department of Chemistry and Biochemistry, Kent State University, Kent, Ohio 44242, United States; oorcid.org/0000-0002-6720-9429; Email: hmao@kent.edu

Authors

Pravin Pokhrel – Department of Chemistry and Biochemistry, Kent State University, Kent, Ohio 44242, United States; orcid.org/0000-0003-4259-6087

Jiayi Wang – Department of Chemistry and Biochemistry, Kent State University, Kent, Ohio 44242, United States

Sangeetha Selvam – Department of Chemistry and Biochemistry, Kent State University, Kent, Ohio 44242, United States

Sagun Jonchhe – Department of Chemistry and Biochemistry, Kent State University, Kent, Ohio 44242, United States; orcid.org/0000-0003-4361-6641

Shankar Mandal — Department of Chemistry and Biochemistry, Kent State University, Kent, Ohio 44242, United States; orcid.org/0000-0002-2653-8760

Complete contact information is available at: https://pubs.acs.org/10.1021/acs.biomac.2c00959

Author Contributions

[†]P.P. and J.W. contributed equally.

Notes

The authors declare no competing financial interest.

ACKNOWLEDGMENTS

H.M. thanks NIH (R01 CA236350) and NSF (CBET1904921) for financial support.

ABBREVIATIONS

RCA, rolling circle amplification; EASE, ensemble assays of single-molecule entities

■ REFERENCES

- (1) Hu, C.; Jonchhe, S.; Pokhrel, P.; Karna, D.; Mao, H. Mechanical unfolding of ensemble biomolecular structures by shear force. *Chem. Sci.* **2021**, *12*, 10159–10164.
- (2) Roy, R.; Hohng, S.; Ha, T. A practical guide to single-molecule FRET. *Nat. Methods* **2008**, *5*, 507–516.
- (3) Kaur, A.; Ellison, M.; Dhakal, S. MASH-FRET: A Simplified Approach for Single-Molecule Multiplexing Using FRET. *Anal. Chem.* **2021**, 93, 8856–8863.
- (4) Neuman, K. C.; Nagy, A. Single-molecule force spectroscopy: optical tweezers, magnetic tweezers and atomic force microscopy. *Nat. Methods* **2008**, *5*, 491–505.
- (5) Carrion-Vazquez, M.; Oberhauser Andres, F.; Fowler Susan, B.; Marszalek Piotr, E.; Broedel Sheldon, E.; Clarke, J.; Fernandez Julio, M. Mechanical and chemical unfolding of a single protein: A comparison. *Proc. Natl. Acad. Sci. U.S.A.* 1999, 96, 3694–3699.
- (6) Li, H.; Oberhauser Andres, F.; Fowler Susan, B.; Clarke, J.; Fernandez Julio, M. Atomic force microscopy reveals the mechanical design of a modular protein. *Proc. Natl. Acad. Sci. U.S.A.* **2000**, 97, 6527–6531.
- (7) Rief, M.; Gautel, M.; Schemmel, A.; Gaub, H. E. The mechanical stability of immunoglobulin and fibronectin III domains in the muscle protein titin measured by atomic force microscopy. *Biophys. J.* **1998**, 75, 3008–3014.
- (8) Eckels, E. C.; Tapia-Rojo, R.; Rivas-Pardo, J. A.; Fernández, J. M. The Work of Titin Protein Folding as a Major Driver in Muscle Contraction. *Annu. Rev. Physiol.* **2018**, *80*, 327–351.
- (9) Rief, M.; Gautel, M.; Oesterhelt, F.; Fernandez, J. M.; Gaub, H. E. Reversible unfolding of individual titin immunoglobulin domains by AFM. *Science* **1997**, *276*, 1109–1112.
- (10) Kellermayer, M. S. Z.; Smith, S. B.; Granzier, H. L.; Bustamante, C. Folding-unfolding transitions in single titin molecules characterized with laser tweezers. *Science* **1997**, *276*, 1112–1116.

- (11) Chen, H.; Yuan, G.; Winardhi, R. S.; Yao, M.; Popa, I.; Fernandez, J. M.; Yan, J. Dynamics of Equilibrium Folding and Unfolding Transitions of Titin Immunoglobulin Domain under Constant Forces. J. Am. Chem. Soc. 2015, 137, 3540–3546.
- (12) De Vlaminck, I.; Henighan, T.; van Loenhout, M. T. J.; Pfeiffer, I.; Huijts, J.; Kerssemakers, J. W. J.; Katan, A. J.; van Langen-Suurling, A.; van der Drift, E.; Wyman, C.; Dekker, C. Highly Parallel Magnetic Tweezers by Targeted DNA Tethering. *Nano Lett.* **2011**, *11*, 5489–5493
- (13) Berghuis, B. A.; Köber, M.; van Laar, T.; Dekker, N. H. Highthroughput, high-force probing of DNA-protein interactions with magnetic tweezers. *Methods* **2016**, *105*, 90–98.
- (14) Ribeck, N.; Saleh, O. A. Multiplexed single-molecule measurements with magnetic tweezers. *Rev. Sci. Instrum.* **2008**, 79, No. 094301
- (15) Bochman, M. L.; Paeschke, K.; Zakian, V. A. DNA secondary structures: stability and function of G-quadruplex structures. *Nat. Rev. Genet.* **2012**, *13*, 770–780.
- (16) Rhodes, D.; Lipps, H. J. G-quadruplexes and their regulatory roles in biology. *Nucleic Acids Res.* **2015**, *43*, 8627–8637.
- (17) Liu, D.; Daubendiek, S. L.; Zillman, M. A.; Ryan, K.; Kool, E. T. Rolling Circle DNA Synthesis: Small Circular Oligonucleotides as Efficient Templates for DNA Polymerases. *J. Am. Chem. Soc.* **1996**, *118*, 1587–1594.
- (18) Ali, M. M.; Li, F.; Zhang, Z.; Zhang, K.; Kang, D.-K.; Ankrum, J. A.; Le, X. C.; Zhao, W. Rolling circle amplification: a versatile tool for chemical biology, materials science and medicine. *Chem. Soc. Rev.* **2014**, *43*, 3324–3341.
- (19) Mao, H.; Luchette, P. An integrated laser-tweezers instrument for microanalysis of individual protein aggregates. *Sens. Actuators, B* **2008**, *129*, 764–771.
- (20) Pokhrel, P.; Sasaki, S.; Hu, C.; Karna, D.; Pandey, S.; Ma, Y.; Nagasawa, K.; Mao, H. Single-molecule displacement assay reveals strong binding of polyvalent dendrimer ligands to telomeric G-quadruplex. *Anal. Biochem.* **2022**, *649*, No. 114693.
- (21) Jonchhe, S.; Selvam, S.; Karna, D.; Mandal, S.; Wales-McGrath, B.; Mao, H. Ensemble Sensing Using Single-Molecule DNA Copolymers. *Anal. Chem.* **2020**, *92*, 13126–13133.
- (22) Dhakal, S.; Cui, Y.; Koirala, D.; Ghimire, C.; Kushwaha, S.; Yu, Z.; Yangyuoru, P. M.; Mao, H. Structural and mechanical properties of individual human telomeric G-quadruplexes in molecularly crowded solutions. *Nucleic Acids Res.* **2013**, *41*, 3915–3923.
- (23) Koirala, D.; Dhakal, S.; Ashbridge, B.; Sannohe, Y.; Rodriguez, R.; Sugiyama, H.; Balasubramanian, S.; Mao, H. A. Single-Molecule Platform for Investigation of Interactions between G-quadruplexes and Small-Molecule Ligands. *Nat. Chem.* **2011**, *3*, 782–787.
- (24) del Villar-Guerra, R.; Trent, J. O.; Chaires, J. B. G-Quadruplex Secondary Structure Obtained from Circular Dichroism Spectroscopy. *Angew. Chem.* **2018**, *130*, 7289–7293.
- (25) Zhou, W.; Suntharalingam, K.; Brand, N. J.; Barton, P. J. R.; Vilar, R.; Ying, L. Possible Regulatory Roles of Promoter G-Quadruplexes in Cardiac Function-Related Genes Human TnIc as a Model. *PLoS One* **2013**, *8*, No. e53137.
- (26) Yu, H.; Gu, X.; Nakano, S.-i.; Miyoshi, D.; Sugimoto, N. Beadson-a-string structure of long telomeric DNAs under molecular crowding conditions. *J. Am. Chem. Soc.* **2012**, *134*, 20060–20069.
- (27) Abraham Punnoose, J.; Ma, Y.; Li, Y.; Sakuma, M.; Mandal, S.; Nagasawa, K.; Mao, H. Adaptive and Specific Recognition of Telomeric G-Quadruplexes via Polyvalency Induced Unstacking of Binding Units. J. Am. Chem. Soc. 2017, 139, 7476–7484.
- (28) Abraham Punnoose, J.; Cui, Y.; Koirala, D.; Yangyuoru, P. M.; Ghimire, C.; Shrestha, P.; Mao, H. Interaction of G-Quadruplexes in the Full-Length 3' Human Telomeric Overhang. *J. Am. Chem. Soc.* **2014**, *136*, 18062–18069.
- (29) Yu, Z.; Koirala, D.; Cui, Y.; Easterling, L. F.; Zhao, Y.; Mao, H. Click Chemistry Assisted Single-Molecule Fingerprinting Reveals a 3D Biomolecular Folding Funnel. *J. Am. Chem. Soc.* **2012**, *134*, 12338–12341.

- (30) Schonhoft, J. D.; Bajracharya, R.; Dhakal, S.; Yu, Z.; Mao, H.; Basu, S. Direct experimental evidence for quadruplex-quadruplex interaction within the human ILPR. *Nucleic Acids Res.* **2009**, *37*, 3310–3320.
- (31) Hardin, C. C.; Watson, T.; Corregan, M.; Bailey, C. Cation-dependent transition between the quadruplex and Watson-Crick hairpin forms of d(CGCG3GCG). *Biochemistry* **1992**, *31*, 833–841.
- (32) Bhattacharyya, D.; Mirihana Arachchilage, G.; Basu, S. Metal Cations in G-Quadruplex Folding and Stability. *Front. Chem.* **2016**, *4*, No. 38.
- (33) Parkinson, G. N.; Lee, M. P.; Neidle, S. Crystal structure of parallel quadruplexes from human telomeric DNA. *Nature* **2002**, *417*, 876–880.
- (34) Wang, Y.; Patel, D. J. Solution Structure of theOxytrichaTelomeric Repeat d[G4(T4G4)3] G-tetraplex. J. Mol. Biol. 1995, 251, 76–94
- (35) Ghimire, C.; Park, S.; Iida, K.; Yangyuoru, P.; Otomo, H.; Yu, Z.; Nagasawa, K.; Sugiyama, H.; Mao, H. Direct Quantification of Loop Interaction and $\pi \pi$ Stacking for G-Quadruplex Stability at the Submolecular Level. *J. Am. Chem. Soc.* **2014**, *136*, 15537–15544.
- (36) Yu, Z.; Gaerig, V.; Cui, Y.; Kang, H.; Gokhale, V.; Zhao, Y.; Hurley, L. H.; Mao, H. Tertiary DNA Structure in the Single-Stranded hTERT Promoter Fragment Unfolds and Refolds by Parallel Pathways via Cooperative or Sequential Events. *J. Am. Chem. Soc.* **2012**, *134*, 5157–5164.
- (37) Evans, E. Probing the relation between force-lifetime-and chemistry in single molecular bonds. *Annu. Rev. Biophys. Biomol. Struct.* **2001**, *30*, 105–128.
- (38) You, H.; Zeng, X.; Xu, Y.; Lim, C. J.; Efremov, A. K.; Phan, A. T.; Yan, J. Dynamics and stability of polymorphic human telomeric G-quadruplex under tension. *Nucleic Acids Res.* **2014**, *42*, 8789–8795.
- (39) Evans, E.; Ritchie, K. Dynamic strength of molecular adhesion bonds. *Biophys. J.* **1997**, *72*, 1541–1555.
- (40) Iida, K.; Majima, S.; Nakamura, T.; Seimiya, H.; Nagasawa, K. Evaluation of the Interaction between Long Telomeric DNA and Macrocyclic Hexaoxazole (6OTD) Dimer of a G-quadruplex Ligand. *Molecules* **2013**, *18*, 4328–4341.
- (41) Niesen, F. H.; Berglund, H.; Vedadi, M. The use of differential scanning fluorimetry to detect ligand interactions that promote protein stability. *Nat. Protoc.* **2007**, *2*, 2212–2221.
- (42) Bell, G. I. Models for the Specific Adhesion of Cells to Cells. Science 1978, 200, 618–627.
- (43) Karna, D.; Pan, W.; Pandey, S.; Suzuki, Y.; Mao, H. Mechanochemical properties of DNA origami nanosprings revealed by force jumps in optical tweezers. *Nanoscale* **2021**, *13*, 8425–8430.
- (44) Koirala, D.; Punnoose, J. A.; Shrestha, P.; Mao, H. Yoctoliter thermometry for single-molecule investigations: A generic bead-on-atip temperature-control module. *Angew. Chem. Int. Ed.* **2014**, 53, 3470–3474.

☐ Recommended by ACS

Real-Time Monitoring of Temperature-Dependent Structural Transitions in DNA Nanomechanical Resonators: Unveiling the DNA-Ligand Interactions for Biomedical A...

Francesca Legittimo, Carlo Ricciardi, et al.

JANUARY 27, 2023

ACS APPLIED NANO MATERIALS

READ 🗹

Probing RNA Conformations Using a Polymer-Electrolyte Solid-State Nanopore

Chalmers Chau, Paolo Actis, et al.

OCTOBER 24, 2022

ACS NANO

READ "

Effect of Flow Rate and Ionic Strength on the Stabilities of YOYO-1 and YO-PRO-1 Intercalated in DNA Molecules

Dinesh Gautam, Jixin Chen, et al.

MARCH 14, 2023

THE JOURNAL OF PHYSICAL CHEMISTRY B

READ 🗹

Tension Gauge Tethers as Tension Threshold and Duration

Jingzhun Liu, Jie Yan, et al.

FEBRUARY 02, 2023

ACS SENSORS

READ 🗹

Get More Suggestions >